



Cite this: *Nanoscale*, 2024, **16**, 2466

Functional magnetic nanoparticles for protein delivery applications: understanding protein–nanoparticle interactions†

Rajat Sharma, ^a Daniel Ungar, ^b Edward Dyson, ^c Stephen Rimmer ^c and Victor Chechik *^a

Iron oxide nanoparticles (IONPs) surface functionalised with thermo-responsive polymers can encapsulate therapeutic proteins and release them upon heating with an alternating magnetic field above the lower critical solution temperature (LCST). In order to make this delivery system clinically-relevant, we prepared IONPs coated with poly-*N*-isopropylmethacrylamide (PNIPMAM), a polymer with LCST above human body temperature. The optimal polymer chain length and nanoparticle size to achieve LCST of *ca.* 45 °C were 19 kDa PNIPMAM and 16 nm IONPs. The PNIPMAM-coated IONPs could encapsulate a range of proteins which were released upon heating above LCST in the presence of a competitor protein or serum. A small amount of encapsulated protein leakage was observed below LCST. The efficiency of protein encapsulation and release was correlated with molecular weight and glycosylation state of the proteins. Magnetic heating resulted in a faster protein release as compared to conventional heating without significant temperature increase of the bulk solution.

Received 8th September 2023,
Accepted 20th December 2023

DOI: 10.1039/d3nr04544g

rsc.li/nanoscale

1. Introduction

Stimuli-responsive nano-assemblies have attracted significant attention, due to their ability to undergo controlled morphological or functional changes.^{1–3,6,8} Heat is a particularly attractive trigger as it can be easily applied either directly with good spatiotemporal control, or indirectly through photothermal or magneto-thermal effects.⁸ Many examples of thermo-responsive polymer assemblies for heat-triggered drug release applications have been reported.^{1–3,8} For instance, some polymers undergo fast and reversible phase transition from a swollen to a collapsed state at the lower critical solution temperature (LCST), which could trigger release of an encapsulated guest molecule. This thermo-responsive behaviour can be combined with magnetic iron oxide nanoparticles (IONPs), which are able to generate heat in the presence of alternating magnetic field (AMF). Polymer-coated IONPs thus can be used to release the encapsulated guest locally at the targeted sites.⁸

The best studied material of this type of application is poly(*N*-isopropylacrylamide) (PNIPAM). However, the LCST of the PNIPAM polymer (*ca.* 32 °C) is below the human body temperature hindering *in vivo* drug delivery application.⁸ The LCST

can be increased by co-polymerisation with hydrophilic monomers such as acrylamide. For instance, poly(*N*-isopropylacrylamide-*co*-acrylamide)-*block*-polyethylene imine coated IONPs provided heat-triggered release of doxorubicin at 39 °C.² Moreover, nanocomposite membranes based on nanogels (LCST *ca.* 40 °C) and magnetite IONPs achieved “on-demand” drug delivery upon the application of an oscillating magnetic field.³ In this case the nanogel was a co-polymer of *N*-isopropylacrylamide, acrylamide and *N*-isopropylmethacrylamide. The latter monomer can also be used to make a homo-polymer, poly(*N*-isopropylmethacrylamide) (PNIPMAM), which has an LCST of *ca.* 42 °C.^{4,5} As PNIPMAM only differs from PNIPAM in one methyl group in its repeat unit, similar drug encapsulation/triggered release behaviour to PNIPAM could be expected.

Most reports on polymer-coated IONPs are focussed on the delivery and release of small molecules.^{6,7} Encapsulation of therapeutic proteins is less explored. Recently, we reported successful protein encapsulation and magneto-thermal release from 10 kDa PNIPAM coated 6 nm IONPs.⁸ With conventional heating, the protein cargo was released above the LCST in the presence of a competitor protein. Importantly, AMF selectively heated the core of IONPs and magnetic heating-triggered protein release could be observed at bulk solution temperatures below the LCST (*ca.* 21 °C). This proof-of-principle study showed successful delivery of the growth factor Wnt3a in a functional form to the mesenchymal stem cells (MSCs). Wnt3a release from coated IONPs resulted in significant increase of cell proliferation.

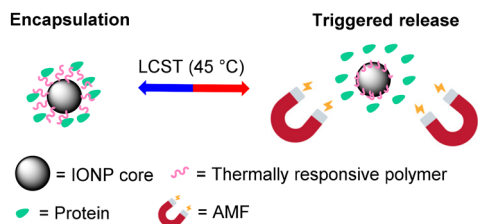
^aDepartment of Chemistry, University of York, UK. E-mail: victor.chechik@york.ac.uk

^bDepartment of Biology, University of York, UK

^cPolymer and Biomaterials Chemistry Laboratories, University of Bradford, UK

† Electronic supplementary information (ESI) available. See DOI: <https://doi.org/10.1039/d3nr04544g>





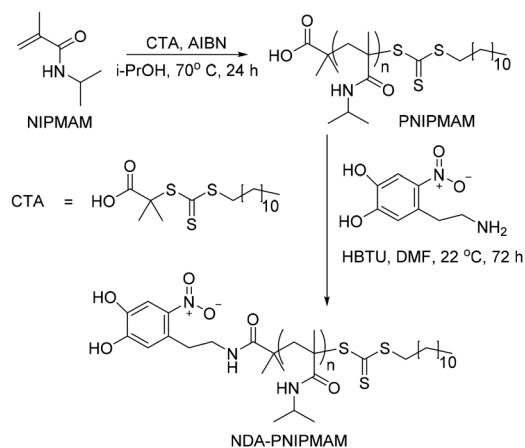
Scheme 1 Schematic illustration of the protein release from the thermally-responsive polymer-coated IONPs using magnetic heating as a trigger.

Here, building on our previous findings, we report construction of PNIPMAM coated IONPs that can release a cargo protein above 45 °C (Scheme 1). The particle size and morphology of IONPs have been optimised to enable efficient heating by AMF. We also show that protein size and glycosylation state are important determinants for encapsulation and competitive release of cargo proteins.

2. Results and discussion

2.1. PNIPMAM synthesis and characterization

Thermally responsive PNIPMAM polymers were synthesized *via* RAFT polymerization with azobisisobutyronitrile (AIBN) as a radical initiator and *S*-1-dodecyl-*S'*-(α,α' -dimethyl- α'' -acetic acid)trithiocarbonate as a chain transfer agent (CTA) (Scheme 2).^{9,10} Polymer with the smallest average molecular weight M_w was characterised by matrix assisted laser desorption ionization mass spectrometry (MALDI-MS) (Fig. 1(i)). The expanded spectrum revealed a repeating set of peaks separated from neighbouring sets by the monomer mass (127 Da), which confirmed the successful synthesis of PNIPMAM. MALDI MS spectra of polymers with higher $M_w > 10$ kDa were too weak. Gel permeation chromatography (GPC) analysis showed that polymer size distribution (Fig. 1(ii)) was broad, presumably



Scheme 2 RAFT polymerization and end group modification to give NDA end group PNIPMAM.

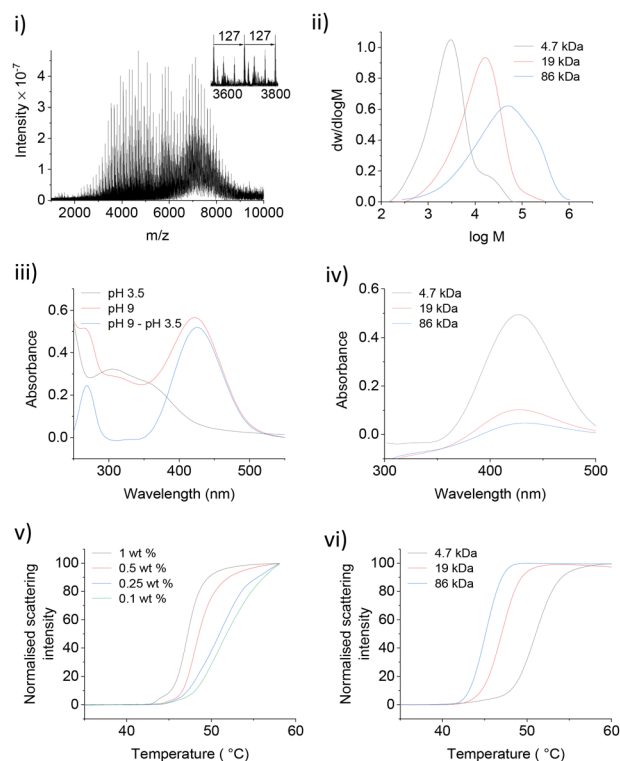


Fig. 1 (i) MALDI-MS spectra of 4.7 kDa NDA-PNIPMAM. (ii) GPC chromatograms of NDA-PNIPMAM. (iii) UV-Vis spectra of 4.7 kDa NDA-PNIPMAM at pH 3.5 and 9 with and without using the pH 3.5 spectrum as a baseline. (iv) UV-Vis spectra of different NDA-PNIPMAM polymers at pH 9 (pH 3.5 as baseline). (v) NanoDSF traces of 19 kDa NDA-PNIPMAM at different concentrations (in 10 mM TRIS, pH = 7). (vi) NanoDSF traces of different NDA-PNIPMAM polymers (0.5 mM in 10 mM TRIS, pH = 7).

due to insufficient removal of oxygen during polymerisation. Nonetheless, both free polymer and polymer-coated nanoparticles showed good phase transition properties in the desired temperature range (*vide infra*).

To facilitate the attachment of PNIPMAM to the IONPs, the end group of the polymer was functionalised with 6-nitrodopamine (NDA), which is a commonly used catechol anchor for iron oxide.¹¹ It can be attached to the PNIPMAM polymer chains either before (pre-functionalisation) or after polymerisation (post-functionalisation).^{12,13} We used the post-functionalisation approach because it allows incorporation of functionalities incompatible with the polymerisation process.¹¹ Functionalisation with NDA was carried out by coupling the acid terminal group of the polymer to the amine functionality of NDA using HBTU as a coupling agent (Scheme 2). MALDI-MS confirmed complete disappearance of the original polymer peaks and the appearance of a new set of NDA functionalized polymer peaks consistent with the conversion of PNIPMAM to NDA-PNIPMAM (Fig. S1.1†).

Since both the thiocarbonylthio and NDA end groups are UV active, the resultant polymer was characterised by UV-Vis spectroscopy (Fig. 1(iii)). The shoulder corresponding to the thiocarbonylthio group (308 nm) confirmed its presence in the



functionalised polymer (Fig. 1(iii)).¹⁴ The UV spectrum of NDA-PNIPMAM showed a nitrocatechol peak at 350 nm (λ_{max}) at acidic pH (below the 1st $\text{p}K_{\text{a}} \approx 7$ of the nitrocatechol group), which shifted to the visible range (*ca.* 422 nm) at pH 9. Free NDA also showed peaks at the same positions. Using a pH 3.5 UV spectrum as a background for the pH 9 spectrum significantly cleans up the nitrocatechol peak at 422 nm (Fig. 1(iv)) which made it possible to quantify NDA functionalisation (Fig. S2.1†). Polymers were further characterised by ¹H NMR (Fig. S3.1†).

Several NDA-PNIPMAM polymers with different chain length were prepared (Table 1). Phase transition behaviour of NDA-PNIPMAM was studied using nano-differential scanning fluorimetry (NanoDSF), which can be used as small-scale turbidimetry. NanoDSF is well-suited for studying LCST as it detects the intensity of scattered light (at 280 nm) as a function of temperature with excellent temperature control. NDA-PNIPMAM showed concentration dependence of its phase transition (Fig. 1(v)). The LCST increased with decrease in the concentration of the polymer sample. This is consistent with literature reports on similar materials.^{15,16} In the literature, LCSTs are usually reported either as the onset of the transition or as the temperature corresponding to the peak rate of scattering intensity change.^{17,18} For our studies, the latter values are reported (Table 1). In addition to the concentration dependence of the LCST, we also observed an increase in the LCST with decreasing PNIPMAM molecular weight (Fig. 1(vi)). This molecular weight dependence of the polymer LCST is also consistent with literature reports.⁴

2.2. PNIPMAM coated IONPs

2.2.1. IONP synthesis. Iron oxide nanoparticles were prepared by adapting literature protocols for thermal decomposition of iron(III) acetylacetonate ($\text{Fe}(\text{acac})_3$) in apolar organic solvents in the presence of ligands (Fig. 2).^{19–22} All nanoparticle batches showed narrow size distributions. IONPs were soluble in organic solvents and hence were stored as toluene solutions at 4 °C.

2.2.2. Ligand exchange of IONPs with NDA-PNIPMAM. IONPs were functionalised with NDA-PNIPMAM using ligand exchange.^{8,11} Excess polymer (in DMF) and IONPs (in toluene) were combined and sonicated for 5 h before stirring them overnight at room temperature. Polymer coated IONPs were purified using ultracentrifugation at 160 000g (22 °C). After purification, the nanoparticles were dispersed and stored in deionised water (dH_2O) at 4 °C. Polymer-coated IONPs showed excellent long-term stability, *e.g.*, no aggregation was observed

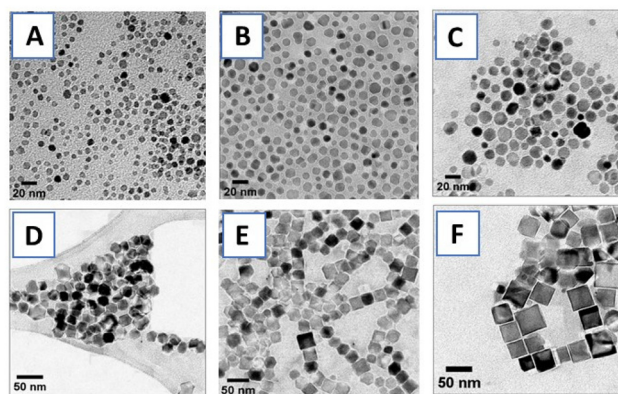


Fig. 2 Representative transmission electron microscopy (TEM) images of IONPs synthesized using thermal decomposition of $\text{Fe}(\text{acac})_3$: (A) 7.3 ± 1.4 nm, (B) 11.0 ± 2.0 nm, (C) 15.4 ± 2.1 nm, (D) 19.1 ± 2.3 nm nano-octahedra, (E) 27.4 ± 3.6 nm and (F) 33.4 ± 4.9 nm nanocubes (\pm denotes standard deviation, $n \geq 100$).

after storage in physiological buffer at room temperature for 6 months (Fig. S4.2†).

PNIPMAM surface coverage of IONPs was estimated by thermogravimetric analysis (TGA) (Fig. 3(i)). Weight loss between 300 °C–450 °C corresponded to the amount of PNIPMAM present on the IONP surface.^{8,11} We observed a gradual increase in the polymer weight loss with decrease in IONP size from 33 nm to 7 nm. For 19 kDa PNIPMAM, the grafting densities for each IONP size were 0.098 chains per nm^2 (7 nm), 0.062 chains per nm^2 (11 nm), 0.058 chains per nm^2 (16 nm), 0.032 chains per nm^2 (19 nm), 0.050 chains per

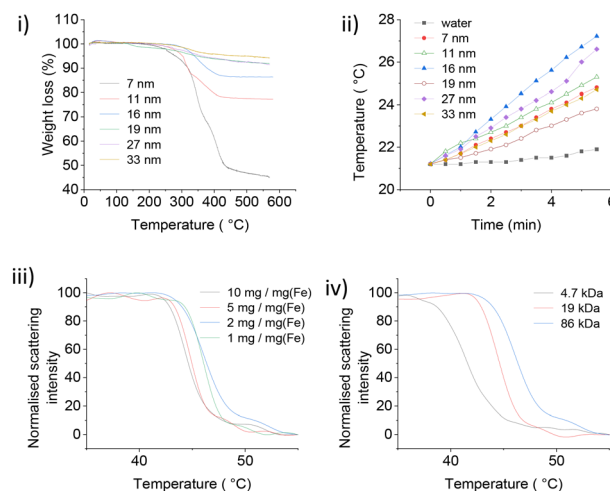


Fig. 3 (i) TGA analysis of 19 kDa PNIPMAM coated IONPs. 20 mg dry PNIPMAM coated IONPs were heated under air at a ramp rate of $10 \text{ }^\circ\text{C min}^{-1}$ between 0–600 °C. (ii) Magnetic heating curves for 19 kDa PNIPMAM @ IONPs. Magnetic heating measurement conditions: 0.45 ml of 10 mg ml^{-1} [Fe], AMF strength of 28.7 mT and frequency of 102.4 kHz. (iii) NanoDSF traces of 16 nm IONPs coated with 19 kDa PNIPMAM. (iv) NanoDSF traces of 16 nm IONPs coated with different chain length polymers. [Fe] = 1 mg ml^{-1} .

Table 1 Different chain length NDA-PNIPMAM synthesized via RAFT polymerization

M_w (kDa)	M_n/M_w	Yield (%)	LCST (°C)
4.7	2.9	70	50.5
19	3.2	80	45.9
86	8.3	76	44.6



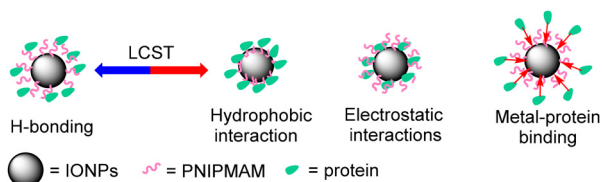


Fig. 4 Different types of protein-IONP interactions.

In order to get some information about the nature of protein-nanoparticle interactions, the effect of particle size and polymer chain length on the encapsulation/release of the model glycoprotein apotransferrin (TRF) was studied. Encapsulation was carried out by suspending the PNIPMAM-coated IONPs and the guest protein in a buffer at 45 °C followed by incubation at room temperature. While loading at high temperature could lead to partial denaturation of the guest protein, we found that this procedure is essential for successful loading and the following release of the protein guest, consistent with our previous observation.⁸ A control experiment with model guest proteins showed no appreciable denaturation under these conditions (Fig. S12.1 and S12.2†).

Protein-loaded IONPs were stable in physiological buffer over a 24 h period. However visible precipitation appeared after 48 h storage, and TEM images showed aggregation after 1 week of storage (Fig. S4.3†). Protein-loaded IONPs were therefore used in subsequent experiments immediately after preparation.

2.4. Protein encapsulation/release studies

2.4.1. Effect of polymer chain length and nanoparticle size on TRF encapsulation/release.

PNIPMAM coated IONPs were loaded with TRF by incubating a solution of protein and nanoparticles above the LCST (45 °C) before gradually cooling to room temperature.⁸ The protein-loaded IONPs were subjected to multiple washes using a solution of the competitor protein RNaseB (10 mg ml⁻¹) below the LCST. This step aimed to eliminate any loosely attached guest protein and minimize subsequent protein leaching from the PNIPMAM coated IONPs. The quantification of protein encapsulation considered both the protein that remained unloaded and that which leached out during the washing process. After encapsulation, heat-triggered release of TRF was studied in the presence of the competitor protein RNaseB at high concentration (10 mg ml⁻¹) to mimic a biological environment, using immunoblotting to quantify protein loading and release.⁸

16 nm IONPs were used as a common core to study the effect of polymer chain length on protein encapsulation and release. TRF encapsulation increased with increasing chain length. When 0.5 mg of PNIPMAM coated IONPs was incubated with 1000 ng of TRF, only minimal protein loading was observed for 4.7 kDa (20 ng). However, as polymer chain length increased, protein encapsulation also increased, reaching 400 ng for 19 kDa polymer, and 700 ng for 86 kDa polymer. Increase in protein encapsulation with increasing

polymer M_w suggests that encapsulation is at least partly driven by the interactions between proteins and polymer chains. After TRF encapsulation, its release was studied at 45 °C in the presence of RNaseB (Fig. 5(i)).

No protein release was observed for 4.7 kDa polymer coated IONPs, however 21 ng TRF was released at 45 °C with minimum leakage at 37 °C for 19 kDa PNIPMAM (Fig. 5(i)).

Further increase in M_w to 86 kDa led to an approximately 2-fold increase in triggered protein release. However, TRF leaching at 37 °C also increased to *ca.* 15 ng. The protein leak at 37 °C could be due to some protein loosely bound to IONPs functionalised with the longest polymer chains. This partial leak at 37 °C indicates the complexity of protein-nanoparticle interactions and underscores the importance of experimental validation of the encapsulation/release system. From these experiments we concluded that the 19 kDa PNIPMAM functionalised IONPs were the most advantageous for our further studies.

The effect of the IONP core diameter on protein encapsulation and release was studied with 7, 11 and 16 nm IONPs. 19 kDa PNIPMAM was used as a common coating and the same amount of IONPs (based on the mass of Fe) was used in these experiments. TRF encapsulation decreased with increasing NP diameter and maximum loading was observed for 7 nm IONPs (*ca.* 900 ng of 1000 ng TRF). This can be readily explained by the high surface area of smaller IONPs.

After TRF loading, we assessed release and found this to be strongly affected by the IONP size (Fig. 5(ii)). Despite higher protein encapsulation, only a small amount of TRF was released from 7 nm (*ca.* 7 ng) and 11 nm (*ca.* 5 ng) IONPs. However, 16 nm IONPs released *ca.* 21 ng at 45 °C with only a slight protein leak observed at 37 °C (*ca.* 1 ng). The smaller particles have higher curvature and hence likely a greater potential for the protein to irreversibly bind to iron oxide, which could be the reason for the observed lower protein release.

In conclusion, protein encapsulation increased with increased polymer chain length and decreased with IONP size. However, only 16 nm IONPs showed an appreciable temperature triggered protein release and hence 16 nm IONPs coated with 19 kDa PNIPMAM were used for all further studies.

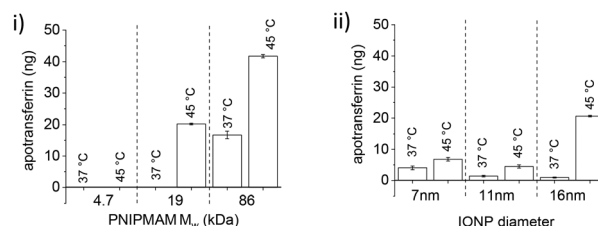


Fig. 5 Effect of (i) polymer chain length with 16 nm IONPs and (ii) IONP diameter with 19 kDa PNIPMAM, on heat-triggered TRF release. Western blot analysis and quantification of TRF release (with 10 mg ml⁻¹ RNaseB) from PNIPMAM coated IONPs at 37 °C and 45 °C (for 1 h), respectively ($n = 3$, error bars denote standard error).



amount of protein leak was approximately three times higher when the larger OVL was used as a competitor (Fig. 7(i)). Heat-triggered GFP release with RNaseB or OVL did not differ significantly from the control experiment at 37 °C, suggesting that the small non-glycosylated GFP protein binds weakly to polymer-coated IONPs. In contrast, IgG's heat-triggered release with OVL as a competitor yielded a similar amount of protein as for TRF (about 150 ng, Fig. 7(ii)). However, there was a significant increase in the IgG leakage at 37 °C with the competitor OVL (*ca.* 30 ng) as compared to RNaseB (*ca.* 10 ng).

Finally, we investigated the kinetics of protein encapsulation by IONPs (Fig. 7(iii)). A range of glycosylated and non-glycosylated proteins used in this study (except GFP) showed similar loading behaviour with the saturation of the binding sites achieved within 60 min. More of the larger and glycosylated proteins was encapsulated as compared to the smaller and non-glycosylated ones, with GFP binding significantly faster than all other tested guest proteins.

Overall, protein encapsulation onto and release from PNIPMAM coated IONP is a complex process which depends on a number of physico-chemical properties of both the guest and competitor proteins. Both below and above the LCST, protein-nanoparticle interactions increased with glycosylation and increasing size of guest or competitor proteins. GFP, a small non-glycosylated protein, binds quickly but leaks out below the LCST, suggesting highly reversible binding.

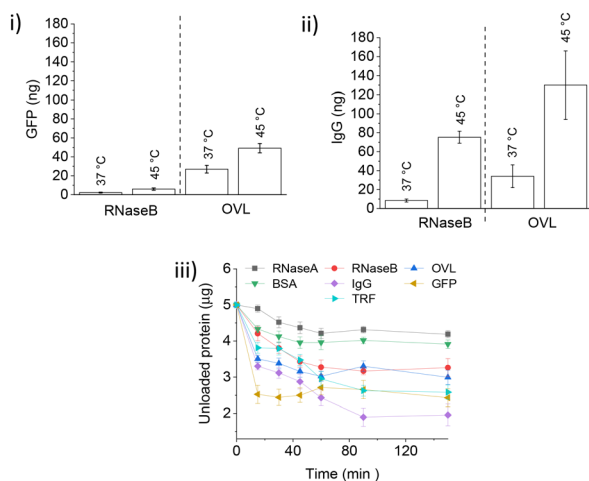


Fig. 7 (i) Heat-triggered release of GFP with different competitors. Quantification of GFP (Fig. S9.1†) release following competitor treatment for 60 min at 37 °C and 45 °C (RNaseB and OVL as indicated) of PNIPMAM coated IONPs loaded with 1000 ng GFP at pH 7.4 ($n = 3$, error bars denote standard error). (ii) Heat-triggered release of IgG with different competitors. Western blot analysis and quantification of IgG (section S10†) release following competitor treatment for 60 min at 37 °C and 45 °C (RNaseB and OVL as indicated) of PNIPMAM coated IONPs loaded with 1000 ng IgG at pH 7.4 ($n = 3$, error bars denote standard error). (iii) Protein encapsulation by IONPs at 22 °C: 0.5 mg PNIPMAM coated IONPs were mixed (350 rpm) with 5000 ng of the protein in the physiological buffer (20 mM HEPES, 100 mM NaCl, pH 7.4) ($n = 3$, error bars denote standard error). Protein quantification was done using Coomassie staining.

2.4.4. Investigating different temperature regimes for encapsulation. Guest protein leak below the LCST is likely to be due to some loosely bound protein. In order to maximise the amount of strongly bound protein and more completely remove the loosely bound guest, we tested different IgG loading/washing conditions (Fig. 8). Mixing PNIPMAM coated IONPs with the guest protein above the LCST (45 °C) for 15 min at the start of the encapsulation process before a 2 h incubation at room temperature was necessary for successful encapsulation, as incubating only at room temperature for 2 h completely eliminated temperature-responsive release above 45 °C (Fig. 8A and B). Importantly though, increasing the initial incubation time at 45 °C to 60 min significantly increased encapsulation, although this also somewhat increased leakage below the LCST (Fig. 8D, E and F). Variation of the length of incubation at 22 °C (following 15 min mixing at 45 °C) up to 2 h did not significantly affect encapsulation/release (Fig. 8B, C and E).

2.4.5. Serum as a competitor for magnetically-triggered IgG release. In any future *in vivo* applications of the coated IONPs, they will be exposed to a cocktail of proteins present in biological milieu.⁴⁰ In order to test whether this will provide a suitable environment for the release of the guest proteins, we explored guest protein release in the presence of serum as a potential source of competitor proteins. In order to quantify the release, we had to use guest proteins whose orthologs in various serums (bovine, goat and pig serum) would not interact with the antibody used for monitoring release (section S11†). For instance, TRF antigens in all three serums were detected by the antibodies used for the detection of human TRF. Hence, TRF release could not be quantified in the release experiments. However, the anti-bovine IgG antibody did not recognise the antibodies present in goat serum (section S11†). This system was therefore used in serum-triggered guest release experiments.

After IgG loading, treatment with goat serum as a competitor (10% in 20 mM HEPES, pH 7.4) during washings resulted in more protein leaching as compared to the OVL washings. The protein release with the serum was somewhat lower than with OVL as a competitor. At 45 °C, *ca.* 70 ng of IgG were released with a significant leakage of *ca.* 40 ng at 37 °C (Fig. 8 (B) and 9(i)). The protein concentration in serum is approxi-

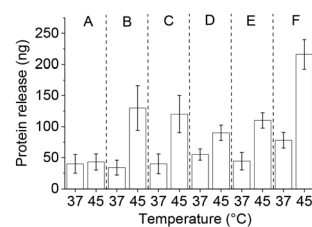


Fig. 8 Triggered IgG release with OVL as a competitor for different protein loading conditions: (A) 2 h at 22 °C (B) 15 min at 45 °C + 2 h at 22 °C (encapsulation procedure used throughout this study), (C) 15 min at 45 °C + 1 h at 22 °C, (D) 5 min at 45 °C, (E) 15 min at 45 °C and (F) 60 min at 45 °C.



dH₂O and separation using Eppendorf centrifugation (20 000g, 30 min at room temperature). The washed precipitates were dissolved in dH₂O (3 ml) and stored at 4 °C. Yield: 20 mg (70%).

4.7. Determination of iron content in the IONPs

Total iron content of IONPs was determined using UV-Vis spectrophotometer.⁴¹ The process was started with dissolving the known weight (5–10 mg) of IONPs in the minimum volume of conc. HCl (0.4 ml), resulting in the formation of a solution containing a mixture of Fe²⁺ and Fe³⁺ ions. The resulted solution was then diluted with dH₂O (25 ml) in a 50 ml volumetric flask and all the iron was then reduced to Fe²⁺ by adding excess of hydroxylamine hydrochloride (4 ml, 10 wt% in dH₂O). To this Fe²⁺ solution, *o*-phenanthroline (4 ml, 0.3 wt% in ethanol) was added resulting in the formation of an orange red complex (pH = 6–6.5) and the content of the iron was determined using the UV-Vis spectrophotometer ($\lambda_{\text{max}} = 511 \text{ nm}$). The standard for the determination of the total iron content was Mohr salt.

4.8. Magnetic heating measurements

The heating performance of the water dispersible IONPs was assessed using an applied alternating magnetic field (magnetic field 28.7 mT, frequency 102.4 kHz, field-frequency product 2884.2 T s⁻¹) at a constant voltage (30.0 V) and current limit (1.95 A). A control experiment checked the background heating of deionised water (dH₂O). 0.45 ml dH₂O was loaded to a sample tube of dimensions 8 mm × 40 mm (diameter × height, Sigma) and the sample was put inside the heating chamber. Sample tube was held in a fixed position by a plastic holder and a lid was adapted to allow for insertion of thin plastic tubing for gallium arsenide thermocouple probe to monitor the temperature changes inside the chamber.⁸ Magnetic heating data for various ligand coated IONPs were then recorded using above described procedure.

4.9. Preparation of protein-loaded nanoparticles

Prior to protein encapsulation, 0.5 mg of polymer-coated nanoparticles (100 μL , 5 mg mL⁻¹ in dH₂O) were washed with 1 ml diethyl ether. Centrifugation (20 000g, 20 min) was used to separate washed IONPs. After ether washing, IONPs were washed three times by suspending in physiological buffer (1 ml) followed by centrifugation (20 000g, 20 min). After washing, IONPs were resuspended in 100 μL physiological buffer containing 1 μg guest protein. The solution was then incubated on a shaker at 45 °C for 15 min to agitate and suspend nanoparticles following precipitation at a temperature above polymer LCST (45 °C). IONPs were then incubated on a shaker at room temperature for 2 h. Particles were then separated using centrifugation, and the supernatant retained as the unloaded protein sample. Particles were then washed by suspending them in 100 μL of 10 mg mL⁻¹ competitor protein solution in physiological buffer and incubating for 1 h at room temperature on a shaker. Particles were then separated using centrifugation and the supernatant was retained as first wash

sample. This washing step was repeated multiple times (7–10), retaining each wash solution for further analysis.

4.10. Protein release assays

0.5 mg of protein-loaded, PNIPMAM coated IONPs were subjected to changes in temperature with or without magnetic heating. Experiments were conducted in 100 μL solutions of 10 mg mL⁻¹ competitor protein in physiological buffer. To study triggered protein release above polymer LCST without magnetic heating, IONPs were resuspended in the competitor protein solution and incubated at 45 °C for 1 h. Between sampling time points IONPs were regularly agitated and at each sampling time point IONPs were magnetically separated before removing 10 μL of the sample volume for analysis. For magnetic heating experiment, pulsed AMF (10 s on–30 s off cycles) was used. 15 μL samples were collected and centrifuged to remove IONPs before collecting 10 μL supernatant for analysis.

4.11. Sample preparation for protein analysis

Following collection, protein samples were made up to 15 μL in SDS-PAGE sample buffer (5% (v/v) glycerol, 50 mM Tris-HCl pH 6.8, 50 mM dithiothreitol (DTT), 1% (w/v) sodium dodecyl sulfate (SDS), 0.7 mM Bromophenol Blue) and boiled at 97 °C for 5 min.

4.12. SDS-PAGE

SDS-PAGE gels were prepared according to the conditions reported in section S12.† For a separating gel composed of 10% (w/v) acrylamide, 375 mM pH 8.8 tris buffer, 0.05% (w/v) ammonium persulfate (APS) and 0.067% (w/v) *N,N,N',N'*-tetramethylethylenediamine (TEMED), and a stacking gel containing 4% (w/v) acrylamide, 125 mM Tris pH 6.8, 0.1% (w/v) APS, 0.1% (w/v) TEMED. Samples were loaded into wells alongside 5 μL of a pre-stained protein ladder (Precision Plus All-Blue, Bio-Rad). Gels were placed in gel tanks and immersed in running buffer (25 mM Tris, 250 mM glycine, 0.1% (w/v) SDS) before running at 100 V constant voltage for 10 min and then at 150 V constant voltage until the dye had reached the bottom of the gel.

4.13. Coomassie staining

Fairbanks Coomassie staining⁴³ was carried out by heating gels in Fairbanks solution A (25% (v/v) isopropanol, 10% (v/v) acetic acid, 0.05% (w/v) Coomassie Brilliant Blue) to boiling before incubation for 5 min then washing with dH₂O. The heating and washing process was repeated with Fairbanks solution B (10% (v/v) isopropanol, 10% (v/v) acetic acid, 0.005% (w/v) Coomassie Brilliant Blue), Fairbanks solution C (10% (v/v) acetic acid, 0.002% (w/v) Coomassie Brilliant Blue) and Fairbanks solution D (10% (v/v) acetic acid). Gels were left in solution D until the background was completely destained. Quantification was carried out using ImageJ software after scanning the gels.



4.14. Western blotting

Western blotting was conducted by semi-dry transfer of gels onto PVDF membranes (Thermo Fisher) for 70 min at 0.3A using 48 mM Tris-HCl, 39 mM glycine, 20% (v/v) MeOH and 0.0375% (w/v) SDS as the transfer buffer. After membrane transfer, different blocking procedures were used for TRF and IgG. For TRF, membranes were blocked using phosphate buffered saline (PBS) with 0.05% (v/v) Tween-20 (PBST) and 5% (w/v) dried fat free milk powder (PBSTM) for 1 h at room temperature. Membranes were then incubated with primary antibody: anti-TRF (1 : 500, Dako) in PBSTM solution overnight at 4 °C. Following six 10 min washes at room temperature in PBSTM solution, goat anti rabbit-horseradish peroxidase (1 : 1000, Bio-Rad) secondary antibody in PBSTM solution was added for 1 h at room temperature. The blot was then washed 3 times with PBSTM solution (5 min each) and 3 times in PBST for 10 min each at room temperature. For IgG, membranes were blocked in tris-buffered saline (TBS) with 0.05% (v/v) Tween-20 (TBST) and Roche blocking solution (1 : 10) for 1 h at room temperature. Membranes were then incubated with goat anti bovine IgG-horseradish peroxidase (1 : 250) for 1 h followed by three 5 min washings with blocking solution followed by three 10 min TBST washings. Blots were imaged on an Invitrogen iBright imaging system after application of Immobilon horseradish peroxidase (HRP) substrate (Millipore). Quantification was carried out using ImageJ software.

Conflicts of interest

There are no conflicts to declare.

Acknowledgements

The authors acknowledge the University of York and Wild fund for funding this project. Dr I. Will (University of York) is gratefully acknowledged for supporting magnetic heating experiments.

References

- J. Zhang and R. D. K. Misra, *Acta Biomater.*, 2007, **3**, 838–850.
- R. K. Dani, C. Schumann, O. Taratula and O. Taratula, *AAPS PharmSciTech*, 2014, **15**, 963–972.
- T. Hoare, J. Santamaria, G. F. Goya, S. Irusta, D. Lin, S. Lau, R. Padera, R. Langer and D. S. Kohane, *Nano Lett.*, 2009, **10**, 3651–3657.
- J. Rathfon and G. Tew, *Polymer*, 2008, **49**, 1761–1769.
- R. Shunmugam and N. G. Tew, *Polymer*, 2005, **43**, 5831–5843.
- M. Giannaccini, M. P. Calatayud, A. Poggetti, S. Corbianco, M. Novelli, M. Paoli, P. Battistini, M. Castagna, L. Dente, P. Parchi, M. Lisanti, G. Cavallini, C. Junquera, G. Goya and V. Raffa, *Adv. Healthcare Mater.*, 2017, **6**, 1601429.
- D. Maity, S. N. Kale, K. R. Ghanekar, M. J. Xue and J. Ding, *J. Magn. Magn. Mater.*, 2009, **321**, 3093–3098.
- M. Walker, I. Will, A. Pratt, V. Chechik, P. Genever and D. Ungar, *ACS Appl. Nano Mater.*, 2020, **3**, 5008–5013.
- R. T. A. Mayadunne, E. Rizzardo, J. Chiefari, J. Krstina, G. Moad, A. Postma and S. H. Thang, *Macromolecules*, 2000, **33**, 243–245.
- J. V. John, C. W. Chung, R. P. Johnson, Y. I. Jeong, K. D. Chung, D. H. Kang, H. Suh, H. Chen and I. Kim, *Biomacromolecules*, 2016, **17**, 20–31.
- S. Kurzhals, R. Zirbs and E. Reimhult, *ACS Appl. Mater. Interfaces*, 2015, **7**, 19342–19352.
- J. S. Kim, T. G. Kim, W. H. Kong, T. G. Parka and Y. S. Nam, *Chem. Commun.*, 2012, **48**, 9227–9229.
- M. Arslan, T. N. Gevrek, J. Lyskawa, S. Szunerits, R. Boukherroub, R. Sanyal, P. Woisel and A. Sanyal, *Macromolecules*, 2014, **47**, 5124–5134.
- K. Skrabania, A. Miasnikova, A. M. B. Koumba, D. Zehm and A. Laschewsky, *Polym. Chem.*, 2011, **2**, 2074–2083.
- C. Boutris, E. G. Chatzi and C. Kiparissides, *Polymer*, 1998, **38**, 2567–2570.
- F. Afroze, E. Nies and H. Berghmans, *J. Mol. Struct.*, 2000, **554**, 55–68.
- K. Otake, H. Inomata, M. Konno and S. Saito, *Macromolecules*, 1990, **23**, 283–289.
- H. G. Schild and D. A. Tirrell, *J. Phys. Chem.*, 1990, **94**, 4352–4356.
- J. Mohapatra, Z. Fanhao, K. Elkins, M. Xing, M. Ghimire, S. Yoon, S. R. Mishra and J. P. Liu, *Phys. Chem. Chem. Phys.*, 2018, **20**, 12879–12887.
- S. Tong, C. A. Quinto, L. Zhang, P. Mohindra and G. Bao, *ACS Nano*, 2017, **11**, 6808–6816.
- D. Kim, N. Lee, M. Park, B. H. Kim, K. An and T. Hyeon, *J. Am. Chem. Soc.*, 2009, **131**, 454–455.
- P. Guardia, R. D. Corato, L. Lartigue, C. Wilhelm, A. Espinosa, M. G. Hernandez, F. Gazeau, L. Manna and T. Pellegrino, *ACS Nano*, 2012, **6**, 3080–3091.
- W. J. Atkinson, I. A. Brezovich and D. P. Chakraborty, *IEEE Trans. Biomed. Eng.*, 1984, **31**, 70–75.
- R. Hergt and S. Dutz, *J. Magn. Magn. Mater.*, 2007, **311**, 187–192.
- U. Gneveckow, A. Jordan, R. Scholz, V. Brüß, N. Waldöfner, J. Rieke, A. Feussner, B. Hildebrandt, B. Rau and P. Wust, *Med. Phys.*, 2004, **31**, 1444–1451.
- H. Mok and M. Zhang, *Expert Opin. Drug Delivery*, 2013, **10**, 73–87.
- P. M. Price, W. E. Mahmoud, A. A. Al-Ghamdi and L. M. Bronstein, *Front. Chem.*, 2018, **11**, 1–7.
- R. K. Dani, C. Schumann, O. Taratula and O. Taratula, *AAPS PharmSciTech*, 2014, **15**, 963–972.
- N. Pandey, J. U. Menon, M. Takahashi, J. T. Hsieh, J. Yang, K. T. Nguyen and A. S. Wadajkar, *Nanotheranostics*, 2020, **4**, 1–13.



- 30 M. A. C. Stuart, W. T. S. Huck, J. Genzer, M. Müller, C. Ober, M. Stamm, G. B. Sukhorukov, I. Szleifer, V. V. Tsukruk, M. Urban, F. Winnik, S. Zauscher, I. Luzinov and S. Minko, *Nat. Mater.*, 2010, **9**, 101–113.
- 31 D. Chakraborty, K. R. Ethiraj and A. Mukherjee, *RSC Adv.*, 2020, **10**, 27161–27172.
- 32 W. J. Jeong, J. Yu and W. J. Song, *Chem. Commun.*, 2020, **56**, 9586–9599.
- 33 N. Zhang, X. Shen, K. Liu, Z. Nie and E. Kumacheva, *Acc. Chem. Res.*, 2022, **55**, 1503–1513.
- 34 M. A. Firestone, S. C. Hayden and D. L. Huber, *MRS Bull.*, 2015, **40**, 760–767.
- 35 M. Ardejani, L. Noodleman, E. Powers and J. Kelly, *Nat. Chem.*, 2021, **13**, 480–487.
- 36 Z. Ghanbari, M. R. Housaindokht, M. R. Bozorgmehr and M. Izadyar, *J. Theor. Biol.*, 2016, **404**, 73–81.
- 37 K. Meng, C. Yao, Q. Ma, Z. Xue, Y. Du, W. Liu and D. Yang, *Adv. Sci.*, 2019, **6**, 1802112.
- 38 J. Prien, D. Ashline, A. Lapadula, H. Zhang and V. Reinhold, *J. Am. Soc. Mass Spectrom.*, 2009, **20**, 539–556.
- 39 L. Lang, R. Couso and S. Kor, *J. Biol. Chem.*, 1986, **261**, 6320–6325.
- 40 M. Leeman, J. Choi, S. Hansson, M. U. Storm and L. Nilsson, *Anal. Bioanal. Chem.*, 2018, **410**, 4867–4873.
- 41 H. Khurshid, J. Alonso, Z. Nemati, M. H. Phan, P. Mukherjee, M. L. F. Gubieda, J. M. Barandiar and H. Srikanth, *J. Appl. Phys.*, 2015, **117**, 17A3371–17A3374.
- 42 H. C. Joao, I. G. Scragg and R. A. Dwek, *FEBS Lett.*, 1992, **307**, 343–346.
- 43 G. Fairbanks, T. L. Steck and D. F. Wallach, *Biochemistry*, 1971, **10**, 2606–2617.
- 44 S. Boune, P. Hu, A. L. Epstein and L. A. Khawli, *Antibodies*, 2020, **9**, 1–20.
- 45 M. Leeman, J. Choi, S. Hansson, M. U. Storm and L. Nilsson, *Anal. Bioanal. Chem.*, 2018, **410**, 4867–4873.

